We are IntechOpen, the world's leading publisher of Open Access books Built by scientists, for scientists

4,800
Open access books available

122,000
International authors and editors

135M
Downloads

Our authors are among the

154
Countries delivered to

TOP 1%
most cited scientists

12.2%
Contributors from top 500 universities

CLARIVATE ANALYTICS BOOK CITATION INDEX INDEXED

WEB OF SCIENCE™

Selection of our books indexed in the Book Citation Index in Web of Science™ Core Collection (BKCI)

Interested in publishing with us?
Contact book.department@intechopen.com

Numbers displayed above are based on latest data collected.
For more information visit www.intechopen.com

2

Thermo-mechanical behaviour of NiTi at impact

Zurbitu[a,c], J.; Kustov[b], S.; Zabaleta[a], A.; Cesari[b], E. and Aurrekoetxea[a], J.
[a]*Mechanical and Industrial Production Department, Mondragon Unibertsitatea, Loramendi 4, 20500 Mondragon, Spain*
[b]*Department of Physics, Universitat de les Illes Balears, Cra Valldemossa, km 7.5, 07122, Palma de Mallorca, Spain*
[c]*Mechanical Design Department, Ikerlan-IK4, Pº. J. Mª. Arizmendiarrieta 2, 20500 Mondragon, Spain*

1. Introduction

The unique properties of NiTi shape memory alloys have been exploited for engineering applications over the last few decades (Funakubo, 1987; Duerig et al., 1990; Otsuka & Wayman, 1998; Auricchio et al., 2001; Lagoudas, 2008). Recently they have become important for impact applications due to their large recoverable strains and high capacity to dissipate energy. For instance, these alloys are highly attractive for impact damping, seismic protection or health monitoring for impact damage detection (Dolce & Cardone, 2001; Tsoi et al., 2003; Qiu et al., 2006). Nevertheless, the thermo-mechanical behaviour of these alloys at impact, deformation rate in the order of 1 - 10^3 s^{-1}, is not yet well known and only a few works deal with the dynamics of the superelastic transformation at impact strain rates, from the parent phase B2 to the martensitic phase B19', studying the mechanical behaviour in compression mode (Chen et al., 2001; Xu et al., 2006), in tensile mode (Zurbitu et al., 2009a), or analyzing the dynamics of propagating phase boundaries (Niemczura & Ravi-Chandar, 2006; Zurbitu et al., 2009b). Unfortunately, there is a lack of knowledge on the thermal evolution of NiTi when it is subjected to impact loads, so this chapter will address this issue. This lack of knowledge is mainly due to the absence of a well-established characterization methodology for this regime (Boyce & Crenshaw, 2005). Nevertheless, it has recently been developed a new methodology based on the conventional instrumented tensile-impact test which is able to obtain mechanical properties of NiTi with high accuracy in the impact range (Zurbitu et al., 2009c).

In the present chapter, a complete characterization of the thermo-mechanical behaviour of superelastic NiTi from low to impact strain rates (10^{-4} -10^2 s^{-1}) is presented. In order to reach this objective, the stress-strain response was simultaneously registered with thermographic observations at different strain rates up to impact, in order to link the evolution of the temperature with the mechanical behaviour. Moreover other conventional techniques such as screw-driven testing machines have also been employed to extend the thermo-mechanical knowledge at lower strain rates.

1.1 Overview of strain rate effect on the mechanical properties of NiTi

It is well known that the stress–induced martensitic transformation is exothermic, whereas the reverse transformation is endothermic. Characteristic stresses and strains of these transformations depend on the temperature, and since the strain rate could change the heat-transfer phenomena, the temperature could vary during the deformation modifying the mechanical response of NiTi (Shaw & Kyriakides, 1995), mainly in terms of transformation stresses or hysteretic behaviour, Fig. 1. The particular interaction between the strain rate, temperature and transformation stress, enhances the sensitivity of the mechanical behaviour to the strain rate, which is a key parameter in the design of impact applications and must be accurately taken into account. So, the knowledge of the strain–rate effects on the thermo-mechanical properties of NiTi is necessary and crucial for the design and optimization of impact applications.

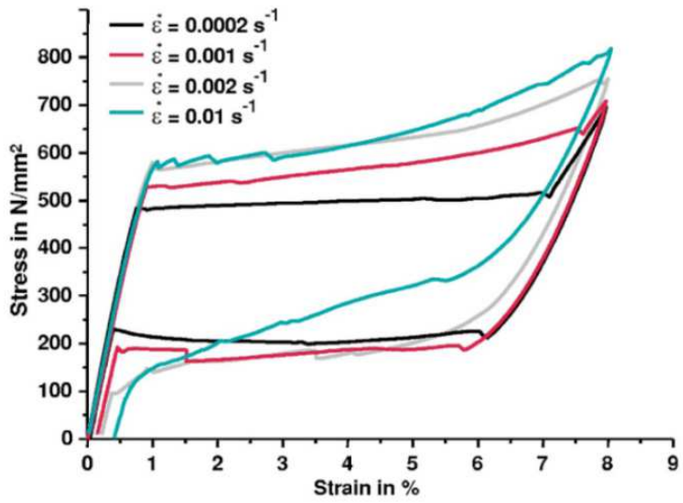

Fig. 1. Stress-strain curves of superelastic NiTi wires with a diameter of 0.9 mm under tension at various strain-rates. [After (Schmidt, 2006)].

Below certain limit, the mechanical behaviour of NiTi is strain rate independent. This is on the order of 10^{-4} s^{-1} (Shaw & Kyriakides, 1995; Schmidt, 2006) and it may be considered as the strain rate limit below which there is enough time to allow all the transformation heat to be completely exchanged with the surroundings. As a result of this feature the temperature does not change in the specimens and the deformation process may be considered as an isothermal one, keeping invariable the mechanical behaviour and constant the transformations stresses.

As the strain rate is raised from the quasi-static limit, the forward transformation stresses increase while the reverse transformation stresses decrease widen then the hysteresis, Fig. 1, as is widely corroborated in the literature (Shaw & Kyriakides, 1995; Vitiello et al., 2005; Schmidt, 2006; Zurbitu et al., 2009a). Above certain strain rate this trend changes, Fig. 2. Thus, the forward transformation stresses stop increasing and become constant after 10^{-1} s^{-1}, and the reverse transformation stresses change their tendency and increase for strain rates higher than 10^{-3} - 10^{-2} s^{-1} (Tobushi et al., 1998; Vitiello et al., 2005; Pieczyska et al., 2006a; Schmidt, 2006; Zurbitu et al., 2009a). The combination of these factors narrows the hysteresis. At high strain rates, the time for heat exchange between the surroundings and

the specimen is reduced so part of the transformation heat is spent in heating up or cooling down the specimen changing the transformation stresses.
It is known that this trend continues until the impact range, **10^{-2}** s^{-1} (Zurbitu et al., 2009a), but it is unknown the temperature evolution at those high strain rates. At impact, the time for heat exchange is drastically reduced and the deformation process is closer to adiabatic conditions, so it is necessary a deeper understanding of the adiabatic nature of the stress induced transformation on the thermo-mechanical behaviour of NiTi.

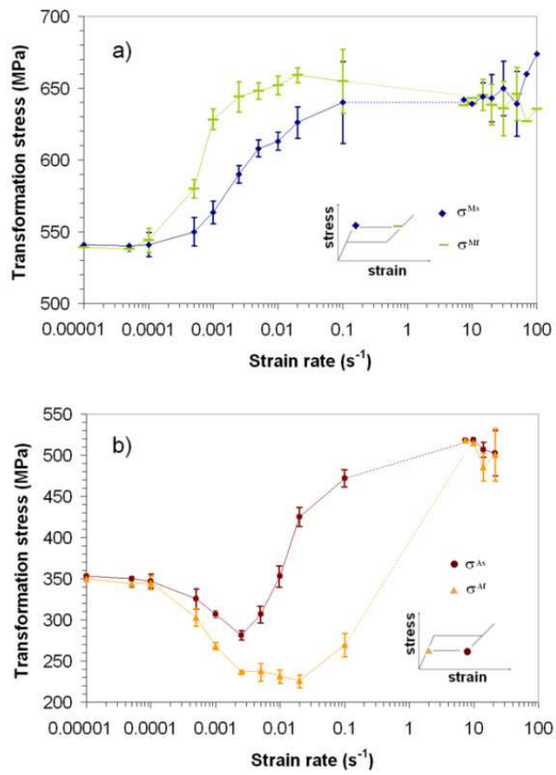

Fig. 2. Variation of the transformation stresses with strain rate: (a) forward SIM transformation stresses, and (b) reverse SIM transformation stresses for a load–unload cycle with complete SIM transformation. [After (Zurbitu et al., 2009a)].

Most of works that study the detwinning of the stress induced martensite in NiTi wires as a function of the strain rate in the tensile configuration, cover the low strain rate range (10^{-5} – 1 s^{-1}) using conventional screw-driven or servo-hydraulic testing machines (Shaw & Kyriakides, 1995; Lin et al., 1996; Wu et al., 1996; Tobushi et al., 1998; Entermeyer et al., 2000; Prahlad & Chopra, 2000; Vitiello et al., 2005; Pieczyska et al., 2006a; Schmidt, 2006). Only a few works deal with the response at very high strain rates in the ballistic range (< 10^{3} s^{-1}), employing the Split Hopkinson Pressure Bar (SHPB) (Miller et al., 2000; Adharapurapu et al., 2006; Bragov et al., 2006). The characterization in the intermediate range (1 – 10^{3} s^{-1}), has been recently possible (Zurbitu et al., 2009a) thanks to the improvement of the conventional instrumented tensile-impact test which is able to measure with high accuracy mechanical properties at impact strain rates (Zurbitu et al., 2009c). Regarding the thermal evolution as a function of the strain rate it is limited to the low range (10^{-5} – 10^{-1} s^{-1}) (Chrysochoos et al., 1995; Li et al., 1996; Chang et al., 2006; Pieczyska et al., 2007), which offers the chance to

study the thermo-mechanical behaviour of NiTi at impact strain rates using the new set up of the conventional instrumented tensile-impact test in combination with thermographic techniques, Fig. 3.

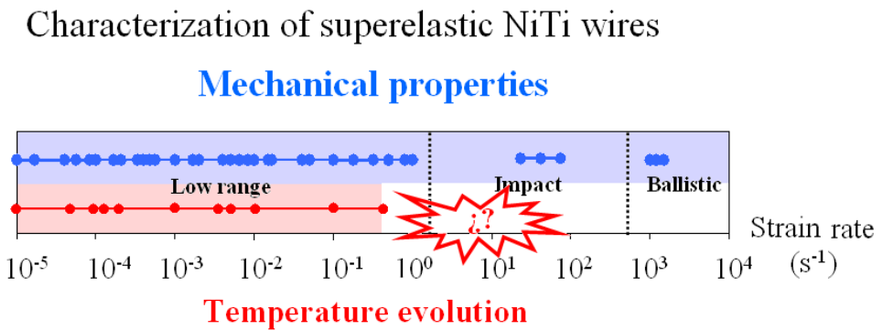

Fig. 3. Overview of the characterization of superelastic NiTi wires as a function of the strain rate

2. Measurement of properties at impact strain rates

2.1 Material: Superelastic NiTi wire

For the experimental work carried out and presented in this chapter it has been chosen a NiTi alloy in the form of wire, 0.5 mm in diameter, showing superelastic behaviour at room temperature, which is commonly used for many researches and applications. Specifically this is a commercially available NiTi wire (ref. NT09), with a nominal composition of 50.9 at.% Ni balanced with Ti, purchased from AMT. The material was supplied in the form of cold drawn wire with a sandblasted surface condition and an average cold worked for 45% based on area reduction with a continuous straight annealing heat treatment at 520 ºC for 30 s in order to optimize the superelastic behaviour. The transformation temperatures deduced from the DSC (Differential Scanning Calorimeter) curves obtained at heating/cooling rates of 10 K/min in the fully annealed condition show that B19′ martensite may be induced by tension at room temperature. (M_f = –51.9 ºC; M_s = –31.4 ºC; A_s = –24.6 ºC; A_f = –6.4 ºC). More detailed information about the material may be found in ref. (Zurbitu et al., 2009a).

2.2 Experimental technique: Stress-Strain-Temperature measurements

In order to obtain the thermo-mechanical properties at impact strain rates some measurements of the stress-strain response and the temperature evolution were taken simultaneously as shows the specially developed experimental set-up of the Fig. 4. This is based on an improved instrumented tensile-impact device (Zurbitu et al., 2009c) which is able to obtain stress-strain measurements with high accuracy at high strain rates, on the order 1-102 s-1. It consists on an impactor which deforms the sample by hitting a mobile grip at which the sample is attached. The impact force is measured by a piezoelectric sensor ICP® quartz force ring attached to the other grip which is fixed. The stress may be easily calculated by dividing the total force by the section of the specimen. The measurement of the strain during the impact was obtained by the integration of the velocity profile of the mobile grip divided by the initial length of the sample. Velocity measurements were carried out with a laser–based non-contacting equipment POLYTEC OFV–505. For the temperature measurements, infrared thermographic pictures were taken at a frame rate of 1250 Hz with a

high speed thermographic camera Flir Titanium 550M during the tensile deformation of the NiTi wires. So, during deformation, simultaneous measurements of infrared radiation, force and velocity were performed so that the temperature is known and the transformation fronts may be visible while it is known the stress-stain state. For the correlation between the transformation stresses and the temperature it is necessary to know not only the emissivity coefficient of the NiTi but also the stress-temperature phase diagram, elements which are detailed below. For the stress-strain-temperature correlation at lower strain rates (10-4 - 10-1 s-1), tests were carried out in conventional screw-driven testing machines INSTRON 4206 and ZWIK Z100 with simultaneous measurement of temperature using the above described thermographic camera.

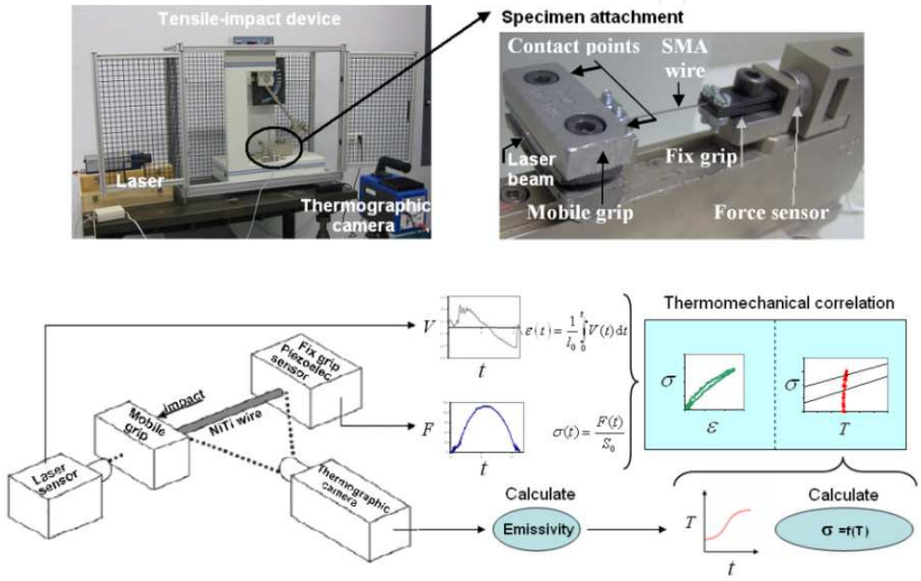

Fig. 4. Experimental set-up for the thermo-mechanical characterization at impact strain rates.

2.3 Emissivity coefficient of NiTi

In the reviewed literature it is possible to find different values of the emissivity coefficient of NiTi, from 0.66 (Iadicola & Shaw, 2007) to 0.83 (Shaw & Kyriakides, 1997). Nevertheless, this value is strongly dependent not only on environmental factors such as the temperature, but also on factors inherent to the material itself such as the composition, roughness, geometry, etc., and therefore it must be calculated for the given testing conditions and the specific material used. Here, for the calculation of the emissivity coefficient of NiTi, samples were employed as described in material section, mounted in the experimental set-up shown in Fig. 3 following the next procedure. On one hand it was measured the temperature of the NiTi wire on the surface by a K-type thermocouple welded to the sample with a high thermal conductivity resin Omegatherm®201. On the other hand a simultaneous thermographic picture of the same area was obtained by means of the thermographic camera described above, and the emissivity value was adjusted until both temperatures match each other. This procedure was repeated for different specimen temperatures achieved by direct Joule effect by passing electric current through the wire ranging from 0.3 to 2A at 0.1 A intervals. The emissivity coefficient that better fits the temperature of the

thermographic data with the thermocouple temperature, within the range from room temperature to 200 ºC, is 0.74, Fig. 5. This emissivity value may be considered relatively high and is due to the roughness of the sandblasted surface finish condition and the superficial oxide layer which increases the emissivity. High values of emissivity minimize the scattering due to the reflections generated by heat sources close to the sample when measuring near room temperatures. It is worth to mention that a constant emissivity coefficient can be only considered under the assumption of a grey body which means that this constant value is only valid for measurements carried out within a certain wavelength interval, limited by the resolution of the thermographic camera which in this case ranges from 3.5 to 5.1 μm.

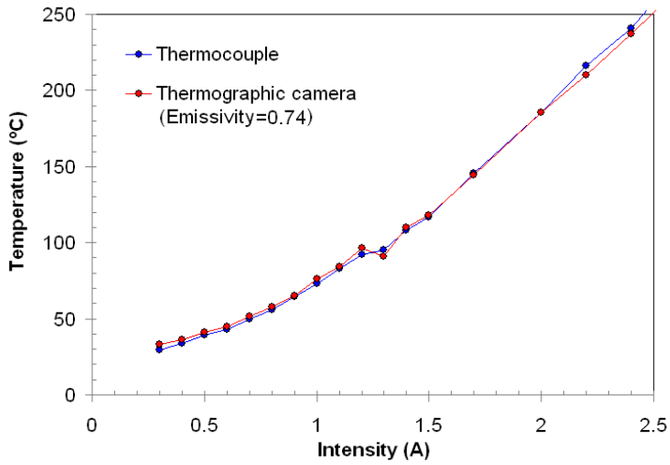

Fig. 5. Adjustment of the emissivity of a NiTi wire with a sandblasted surface condition.

2.4 Stress-temperature phase diagram

By means of the phase diagram shown in Fig. 6(a) it is possible to determine the phase of the material as function of the stress and temperature. This diagram may be used for the thermo-mechanical correlation between the properties obtained from tensile tests, such as the transformation stresses, and the evolution of the temperature. The phase diagram was built based on stress-strain tests with complete stress induced martensitic transformation at different temperatures, Fig. 6(b). The transformation stresses were obtained from these tests at 3% in strain during the forward transformation, and at 2.5% during the reverse one. These tests were carried out in a conventional screw-driven testing machine equipped with climatic chamber. For the correct determination of the phase diagram it is necessary to ensure that the specimen temperature is homogeneous and the same than that kept by the climatic chamber. For this, the tests were conducted under strain controlled conditions at a uniform strain rate of 10^{-4} s^{-1}, low enough to ensure that all the transformation heat is removed from the sample to the surroundings and grips keeping the temperature in the sample stable. The temperature dependence of transformation stresses is given by the Clausius-Clapeyron equation 1, where C_M (forward transformation) and C_A (reverse transformation) are constants and calculated by linear regression as 5.9 and 6.7 $MPa \cdot K^{-1}$ respectively for the alloy here employed.

$$\frac{d\sigma_M}{dT} = C_M ; \frac{d\sigma_A}{dT} = C_A \tag{1}$$

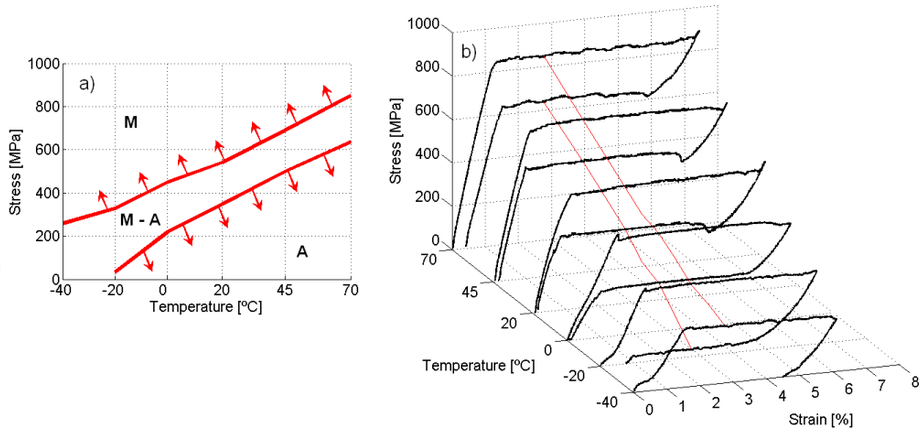

Fig. 6. Stress-temperature phase diagram of NiTi (a), obtained from stress-strain tests with complete stress induced martensitic transformation at different temperatures (b).

3. Thermo-mechanical behaviour of NiTi at impact strain rates

Thanks to the experimental set-up shown in Fig. 4, the determination of the emissivity coefficient of the NiTi and the stress-temperature phase diagram, it is possible to obtain the thermo-mechanical response of NiTi at high strain rates. As a summary of the results obtained, these have been divided into three basically different types of behaviour, a) elastic deformation of the austenitic phase, b) stress induced martensitic transformation and c) elasto-plastic deformation of the martensitic phase.

3.1 Elastic deformation of the austenitic phase at impact

In this case NiTi wire specimens as described above, of 79 mm in length were used. Tests were carried out with an impactor mass of 1.098 kg at an impact velocity of 0.35 m/s corresponding to a strain rate of 4.4 s^{-1}. The force-time graph shown in Fig. 7(a) suggests an elastic deformation of the austenitic phase, which is supported by the stress-strain curve of the Fig. 7(d). Regarding the strain-rate evolution during the impact tests, Fig. 7(d), it keeps close to the initial one during most part of the test and only differs considerably at the highest strain, where the velocity must pass by zero in order to perform the unloading. The very small hysteretic loop observed in the stress-strain curve of the Fig. 7(d) could be due in part to the rearrangement of a certain amount of R-phase variants transformed from the austenitic phase at lower stresses than the stress-induced B19′ martensitic phase (Zurbitu et al., 2009a). The austenite/R-phase transformation is almost negligible in terms of dissipated energy when it is compared with the stress-induced B19′ transformation, but it is visible in Fig. 7(d) as a small slope variation around 0.5% in strain and a small hysteresis. Moreover, during the deformation, small defects may arise even at the elastic range due to the high strain rates. This may explain the small plastic strain after the test shown in Fig. 7(d). Regarding the evolution of temperature, Fig. 7(c), it increases slightly during the loading path because of the small heat generated during the parent phase/R-phase transformation that cannot be released from the specimen due to the high strain rate. During the unloading path, the temperature decreases due to the endothermic character of the retransformation to the austenitic phase, but the small heat generated by defects is kept in the material so the

temperature-time curve is not symmetrical and is slightly offset, Fig. 7(c). Comparing the stress and temperature evolution together with the phase diagram, Fig. 7(e), it is shown that the stress just reaches that necessary to induce the martensitic transformation but it does not transform.

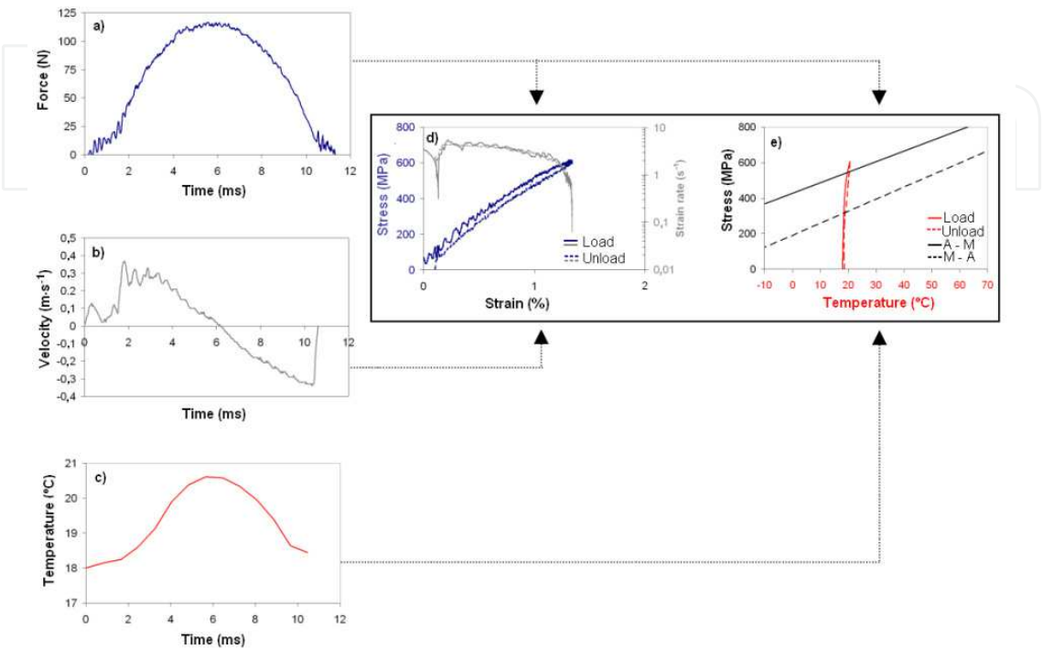

Fig. 7. Elastic deformation of the austenitic phase of NiTi at impact strain rates, a) force-time, b) velocity-time, c) temperature-time, d) stress-strain and strain rate, e) stress-temperature.

3.2 Stress induced martensitic transformation at impact

Here the impactor mass and the initial length is the same than in the previous case, but the impact velocity increases to 1.21 m/s corresponding to a strain rate of 15 s^{-1}. The experimental results show that at impact strain rates, it is still possible to induce the martensitic transformation in NiTi wires, Fig. 8(a). When the force is high enough (b_1), the austenitic lattice becomes thermodynamically unstable being the energy necessary to induce the martensitic transformation lower than that necessary to continue with the elastic deformation of the martensitic phase. Here is shown that at impact the detwinning process occurs at a constant force (b_1 – b_2) as is shown in (Zurbitu et al., 2009a), similarly than that observed at very low strain rates (Shaw & Kyriakides, 1995). From the point (b_2) almost all the specimen consist on detwinned martensite and the strain goes on with the elastic deformation of this phase increasing the force. Once the maximum force is achieved (b_3), the elastic unloading of the martensitic phase begins up to (b_4). Here the martensitic phase becomes unstable and the material transforms back to the parent phase also at a constant force (b_4–b_5). At (b_5) all the martensitic phase is transformed into austenite and the elastic unloading of the austenitic phase takes place. Once the force is removed, most of the deformation is recovered but it may be observed a small portion of permanent deformation, Fig. 8(d), due to the increment of dislocation density and slips occurred during deformation of the martensitic phase. Similarly to that observed at very low strain rates (Liu et al., 2002),

the slope of the beginning of the elastic deformation of the martensitic phase is smooth since there is a portion of residual austenite which needs a continuous increment of force to be transformed. The elastic modulus of martensite is higher during unloading than during loading. This is due to the differences in deformation mechanisms. During unloading, the elastic recovery of the martensitic phase prevails, while during loading, not only elastic deformation of martensite but also strain hardening and residual transformation of austenite occurs.

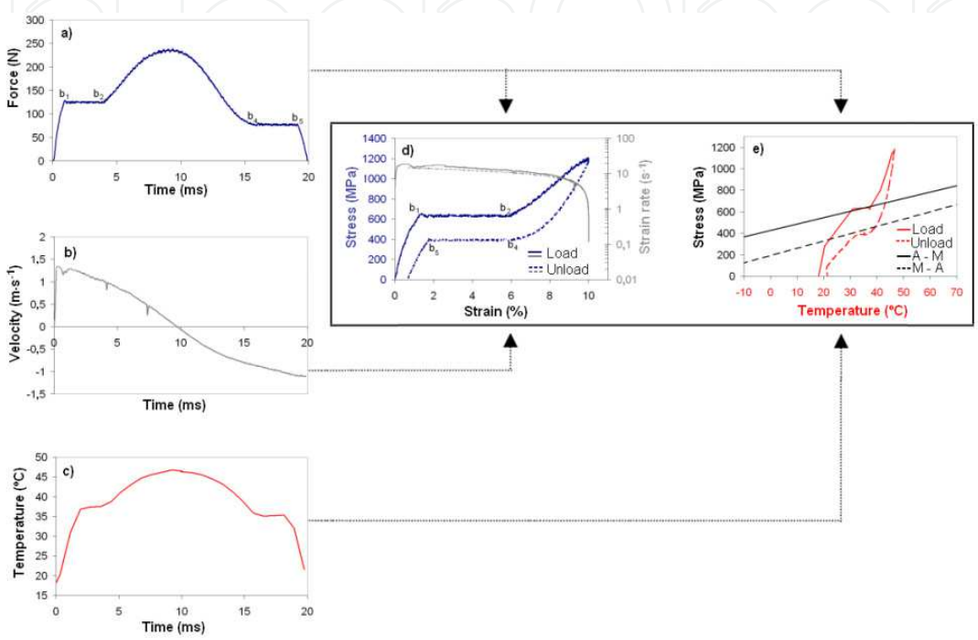

Fig. 8. Stress induced martensitic transformation at impact strain rates, a) force-time, b) velocity-time, c) temperature-time, d) stress-strain and strain rate, e) stress-temperature.

During the transformation, the temperature in the martensitic phase may be up to 20ºC higher than the initial one, Fig. 8(c). As a result of this feature, the transformation stresses are higher at impact than at quasi-static strain rates, where the temperature remains unchanged during the deformation, Fig. 9. This is due to the inherent sensibility of the characteristic transformation stresses to the temperature in NiTi, as establishes the Clausius-Clapeyron relationship shown in equation 1. During the deformation at very low strain rates, the transformation heat may be removed from the sample to the surroundings and grips, and the temperature keeps constant during the transformation. In this case, the deformation may be considered as an isothermal process. When the strain rate increases up to impact levels, the time necessary to remove the transformation heat is so reduced that the deformation process may be considered closer to the adiabatic conditions, and the most part of the heat generated during the forward exothermic transformation is spent in warming up the sample raising the transformation stresses.

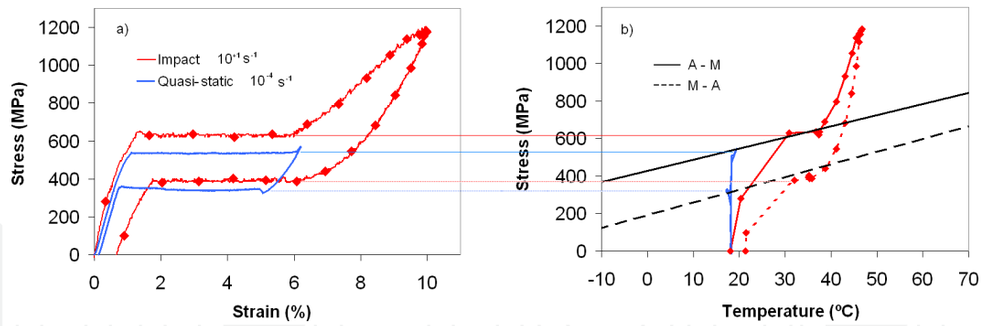

Fig. 9. Correlation between the transformation stresses and temperature stresses for different strain rates.

In the theoretical case of fully adiabatic deformation, the rise in temperature ΔT should be 29.1ºC, equation 2, where C_e is the specific heat of NiTi (data provided by the manufacturer) 490 J kg^{-1} K^{-1}, and $\Delta H_{A\text{-}M}$ the transformation enthalpy, 14.25 kJ kg^{-1}, obtained from measurements at a heating/cooling rate of 10 K/min. Comparing the theoretical temperature variation with the experimental one, it is observed that, in fact, the deformation process at impact strain rates is close to adiabatic conditions.

$$\Delta T = \frac{\Delta H_{A-M}}{c_e} \tag{2}$$

According to the value obtained for the sensibility of the forward transformation stresses with the temperature applying the Clausius-Clapeyron relationship, C_A=5.9 MPa·K^{-1}, the theoretical stress increment corresponding to a 20ºC variation is 114 MPa. This value is very close to the experimental measurements obtained from tests like those of the Fig. 9, which is 120 ± 10 MPa.

3.3 Elasto-plastic deformation and failure of the martensitic phase at impact

Increasing the impact energy, the elastic deformation of the stress induced martensitic phase continues up to the failure instead of the unloading, Fig. 10. In this case the impactor mass is the same than in the previous cases but the impact velocity **is** raised up to 1.63 m/s. The sample initial length was 31 mm so the corresponding strain rate was 53 s^{-1}. Following the transformation at constant force, Fig. 10(a) (d_1–d_2), the strain continues with the elastic deformation of the martensitic phase (d_2–d_4) together with the residual transformation of austenite (d_2–d_3) as is shown in the previous section. In (d_4–d_5) the stress is so high that the dislocation density and slips increase as is evidenced by the strain-hardening shown in the stress-strain diagram of the Fig. 10(d). Finally, the stress decrease from point d_5 suggests necking before failure. For this higher strain rates, on the order of 10^2 s^{-1}, both the rise in temperature during the transformation (18ºC), Fig. 10(c), and the stress increment respect to the quasi-static case (125 MPa), are similar that at lower impact strain rates, 1-10 s^{-1}. So in the strain rate range studied the fact of an increase of the strain rate does not involve further increases in temperature or stresses during the transformation. This means that once the deformation process reaches the quasi-adiabatic condition, the efficiency of the transformation heat in warming the sample reaches the maximum. So, it may be considered that further increments of strain rate will not cause further increases of temperature or transformation stresses; at least while the deformation mechanism remains unchanged.

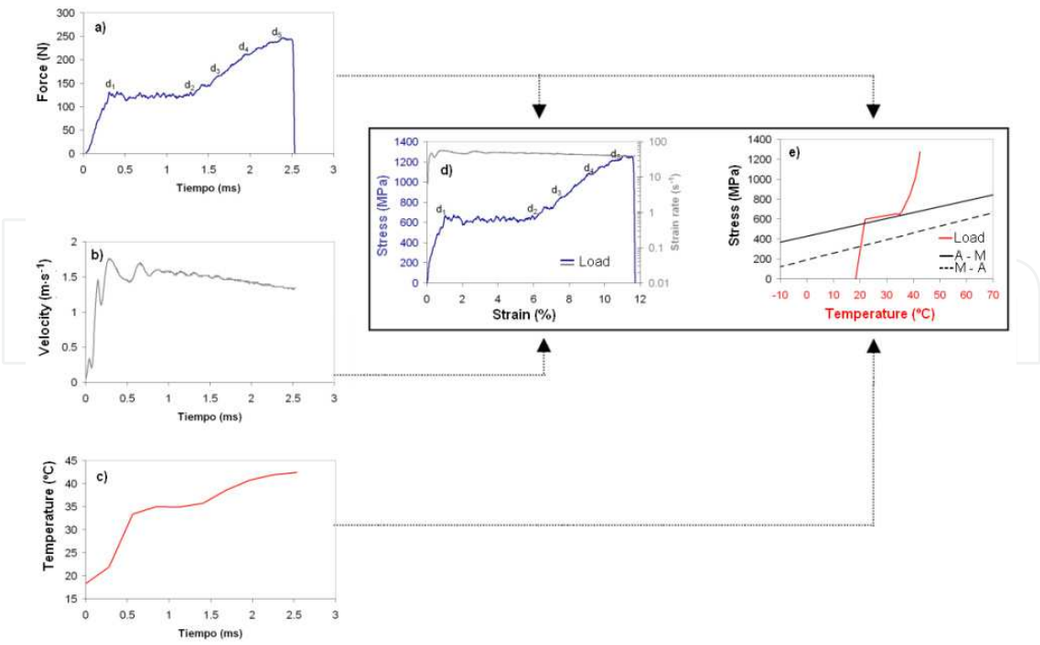

Fig. 10. Elasto plastic deformation of the stress induced martensitic phase at impact strain rates, a) force-time, b) velocity-time, c) temperature-time and strain rate, d) stress-strain and strain rate, e) stress-temperature.

4. Thermo-mechanical behaviour of NiTi at lower strain rates

Below the isothermal strain rate limit, on the order of 10^{-4} s^{-1} for NiTi, the temperature remains unchanged so that the transformation stresses do not vary during deformation as is shown in Fig. 9 and corroborated by other authors (Shaw & Kyriakides, 1995). At higher strain rates, the forward transformation stresses, σ^{Ms} and σ^{Mf}, increase due to the rise in temperature, while the reverse ones, σ^{Ms} and σ^{Mf}, decrease due to the lower temperatures reached in the sample, Fig. 11. The reason of this behaviour is widely supported in the literature (Shaw & Kyriakides, 1995; Wu et al., 1996; Tobushi et al., 1998; Liu et al., 2002). When the strain rate increases, the time necessary to allow the transformation heat exchange with the surroundings is reduced. Thus, a fraction of the heat generated during the exothermic forward transformation remains in the sample increasing **its** temperature and hence the transformation stresses. In the same way, during the endothermic reverse transformation, part of the heat absorbed is transferred from the sample diminishing **its** temperature and the characteristic transformation stresses.

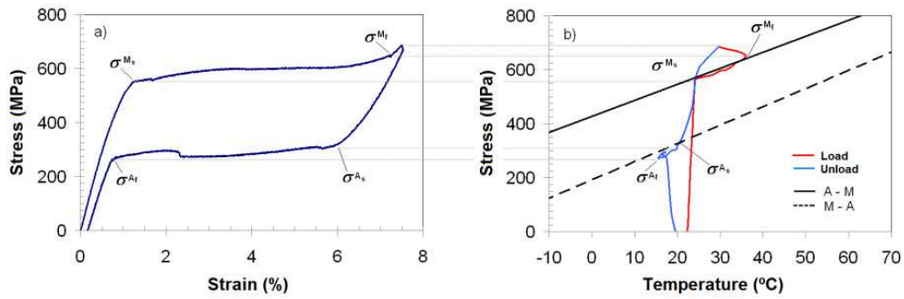

Fig. 11. Thermo-mechanical behaviour of NiTi deformed at a strain rate of 10^{-3} s^{-1}, a) stress-strain diagram, b) temperature evolution of the transformation zone.

The higher the strain rate is, the greater this effect is, Fig. 12, since the time for heat exchange is reduced even further. The stress variation is more pronounced at the end than at the beginning of the transformations because the temperature of the transformation zone increases as the transformation progresses. This causes an increase in the slope of the stress-strain diagram. On the other hand, as the strain rate increases it becomes more evident the residual transformation zone which requires an increase in the external load to be transformed, Fig. 12. The temperature evolution shown in these zones suggests that the residual transformation really occurs, because the temperature continues increasing or decreasing during the residual transformations while during the elastic deformation the evolution of the temperature changes since the heat input/absorption of heat stops. It is worth mentioning that the small stress peaks shown during transformations in the stress-strain diagram of the Fig. 12 are related with new nucleations of the martensitic phase. This aspect is further discussed in the next section.

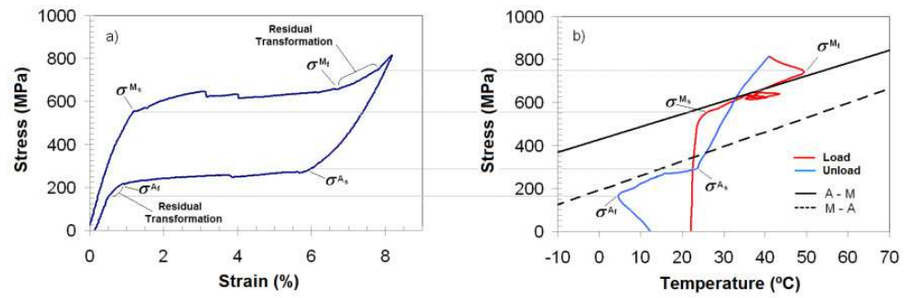

Fig. 12. Thermo-mechanical behaviour of NiTi deformed at a strain rate of $5x10^{-3}$ s^{-1}, a) stress-strain diagram, b) temperature evolution of the transformation zone.

It is known that there is a strain rate value, around 10^{-1} s^{-1} (Zurbitu et al., 2009b), above which this parameter seems to have little influence over the forward transformation stresses. Here is shown that at this strain rate, the temperature reached during the forward transformation, Fig. 13(b), is similar to that observed at impact, with strain rates two orders of magnitude higher, Fig. 9(b). Thus, above 10^{-1} s^{-1}, the deformation process during loading may be considered close to adiabatic conditions and the forward transformation stresses are not influenced by strain rate, Fig. 14.

Regarding the reverse transformation, it is also well known that characteristic transformation stresses change their decreasing tendency and rise above certain strain rate located around 10^{-3} - 10^{-2} s^{-1} (Schmidt, 2006; Zurbitu et al., 2009b). Here is shown that this is due to the higher temperatures developed during the unloading, Fig. 13(b). While at lower strain rates there is enough time to cool the specimen during the elastic recovery of the martensitic phase up to the initial temperature, Fig. 11 and Fig. 12, at 10^{-1} s^{-1}, the time is so reduced that the temperature at the beginning of the reverse transformation is clearly higher than the initial one so the stresses are higher too, Fig. 13. At this strain rate, the temperature along the reverse transformation is reduced decreasing thus the stress. Nevertheless, at impact, the reverse transformation stress keeps constant along the whole reverse transformation, Fig. 14, since the temperature keeps also constant during the process, Fig. 9(b).

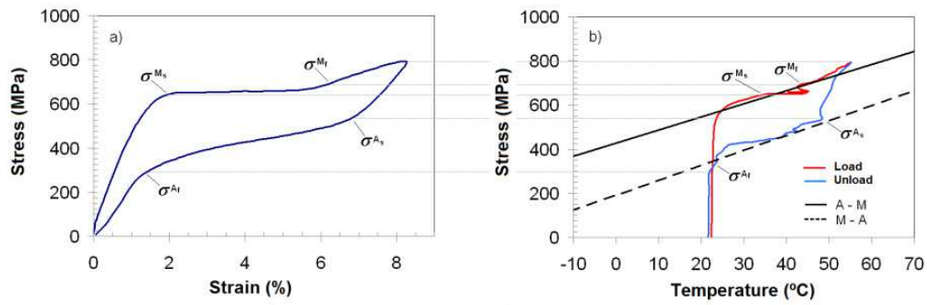

Fig. 13. Thermo-mechanical behaviour of NiTi deformed at a strain rate of 10^{-1} s^{-1}, a) stress-strain diagram, b) temperature evolution of the transformation zone.

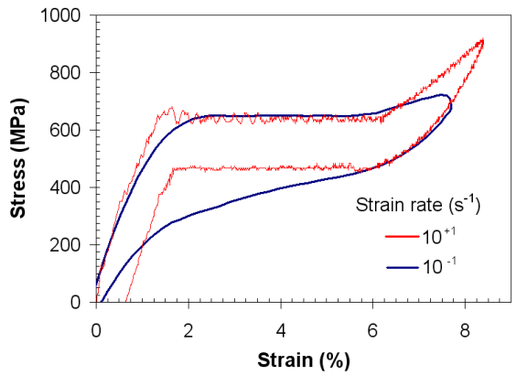

Fig. 14. Stress-strain behaviour of NiTi at different strain rates.

5. Nucleation and phase transformation front evolution

The martensitic transformation occurs by the nucleation and propagation of phase transformation fronts. This inhomogeneous deformation mode divides a deformed sample into transformed and non-transformed zones; and is in this interface, the phase transformation front, at which the lattice distortion takes place. It is well known that the evolution of the amount of transformation fronts strongly depends on the strain rate, at least for the low strain rate range (Leo et al., 1993; Shaw & Kyriakides, 1995), nevertheless the dynamics of the transformation is unknown when it is induced at impact strain rates.

The progress of phase transformation fronts may be observed in many different ways, e.g. by means of strain gauge measurements at different locations (Shaw & Kyriakides, 1995), or measuring changes in temperature along the sample length. The exothermic/endothermic character of the forward/reverse SIM transformation changes the local temperature making visible the nucleation and propagation of phase transformation fronts. This information may be obtained in several ways, by means of small contact thermocouples (Shaw & Kyriakides, 1995), or by means of thermographic pictures (Shaw & Kyriakides, 1997). The latter technique is able to capture the temperature of a greater number of points, so that the resolution in regard to the nucleation and evolution of the phase transformation fronts is higher.
In any of cases, the maximum strain rate at which these tests may be carried out, is directly related to the maximum sampling rate of the measurement systems. In the most recent works, the maximum strain rate at which phase transformation fronts have been observed via thermographic pictures is on the order of 10^{-1} s^{-1} (Pieczyska et al., 2006b), and only a few groups have studied the dynamics of the martensitic transformation at impact monitoring the strain with strain gauges (Niemczura & Ravi-Chandar, 2006). Nevertheless, there is a lack of experimental data on the measurements of the evolution of the phase transformation fronts at impact together with the stress-strain state.
The experimental set-up presented in Fig. 4 enables to obtain temperature measurements along the sample at different moments when it is deformed at impact strain rates, on the order of 10^{1}-10^{2} s^{-1}, while it is known the stress-strain state. The observation of the phase transformation fronts at impact could help in providing a better understanding of the stress induced martensitic transformation at high strain rates. Moreover, the use of the infrared thermographic technology simultaneously with conventional testing machines, allows the observation of fronts in the range of low strain rates, 10^{-4}-10^{-1} s^{-1}, which extends the understanding of the martensitic transformation as a function of the strain rate.

5.1 Phase transformation fronts evolution at impact strain rates

First of all it has been observed the evolution of the phase transformation fronts at impact for a complete martensitic transformation restricting the maximum strain achieved during deformation in order to avoid the elasto-plastic deformation of the martensitic phase, which may cause defects in the crystal lattice. For this, thermographic pictures were taken each 0.8 ms along a NiTi wire deformed up to 6.5% at a strain rate of 10 s^{-1}, Fig. 15(a). While the austenitic phase remains at nearby ambient temperature, the martensitic phase temperature rises due to the exothermic character of the forward transformation. During the unloading, the endothermic character of the reverse transformation cools again the austenitic phase to room temperature while the martensitic phase remains at higher temperature since the high speed of the impact event makes unable the releasing of the transformation heat from this phase. Then, the temperature difference between the austenite phase (low temperature) and martensite phase (high temperature) makes clearly visible the phase transformation fronts and their evolution in Fig. 15.

After the elastic deformation of the austenitic phase, the nucleation of the martensitic phase takes place at both ends of the sample near the grips, where stress concentrations are unavoidable. As the strain is increased, the two transformation fronts progress along the sample until completing the transformation. During unloading, the reverse transformation

takes place at points where the forward transformation was finished. The confluence of the forward transformation fronts originates a discontinuity in the crystal lattice which is favourable for the nucleation of reverse transformation.
At impact no more nucleations were observed so that only the phase transformation fronts arising from the mentioned nucleations appear. This feature shows that the martensitic transformation at impact is inhomogeneous, similarly to that observed at very low strain rates, on the order of 10^{-4} s^{-1}, when the deformation may be considered as an isothermal process (Shaw & Kyriakides, 1995), going against the trend shown in some works (Shaw & Kyriakides, 1997; Chang et al., 2006), where the phase transformation fronts are multiplied as the strain rate is increased in the range 10^{-4} - 10^{-2} s^{-1}. This change of trend will be discussed in the next section.

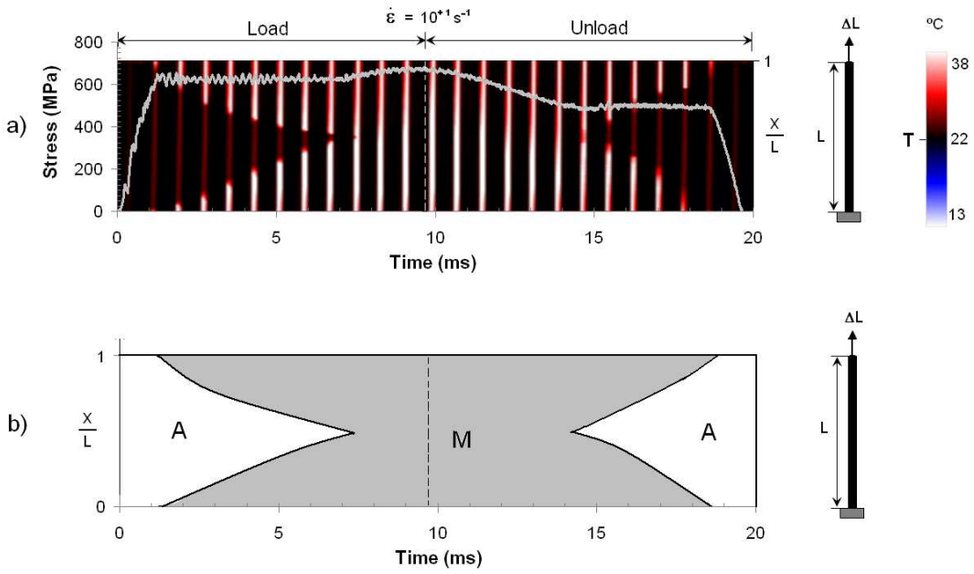

Fig. 15. a) Simultaneous evolution of the phase transformation fronts and the stress during an impact test (ε_{max}=6.5%), b) schematic phase diagram A(austenite)-M (martensite).

With the aim to study in depth the progress of the transformation, the temperature profiles measured along the central axis of the wire for each thermographic picture of the Fig. 15(a) were measured. Each of these profiles, represented by black lines in Fig. 16(b and c), correspond to a specific stress-strain state during the transformation Fig. 16(a), and they form a three-dimensional image that represents the gradient of temperatures between phases and the evolution of transformation fronts.
The short time during deformation at impact, on the order of a few milliseconds, makes unable to reach a steady state in the distribution of the temperature along the sample. The deformation time is so reduced that the heat transfer is confined to a small area between phases while the already transformed region remains at a higher temperature because the heat cannot be released to the surroundings or to other zones of the sample. This leads to a transient regime which shows a temperature gradient between the phases.

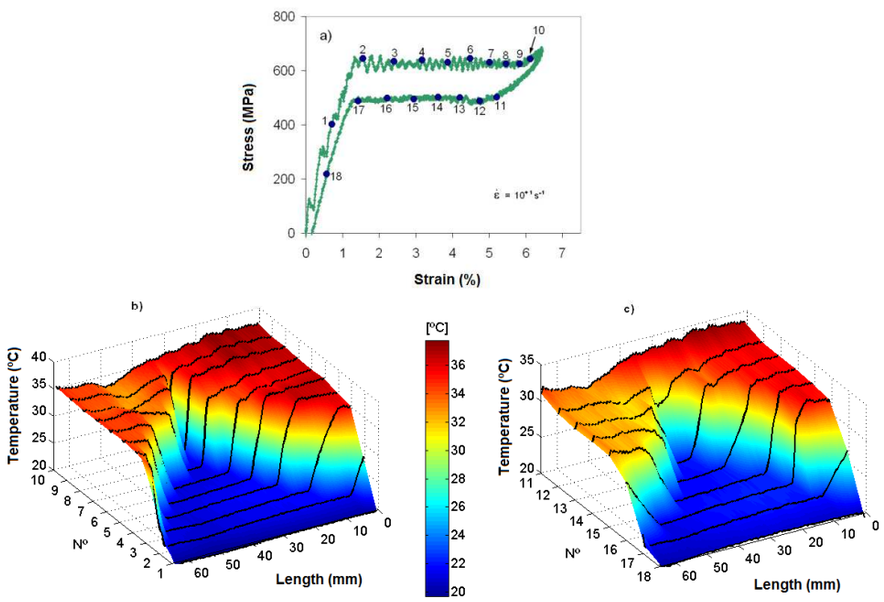

Fig. 16. Evolution of the complete stress induced martensitic transformation at impact strain rates, a) stress-strain diagram, b) temperature evolution during the forward transformation, b) temperature evolution during the reverse transformation.

When the deformation is high enough to induce the elasto-plastic deformation of the martensitic phase, some defects may arise in the crystal lattice modifying the evolution of the reverse transformation. The small stress fields formed around defects during loading may retain certain amount of preferential oriented martensite that lowers the stress necessary to perform the reverse transformation during the unloading and assisting the generation of new nucleations. This effect is shown in Fig. 17, that besides the first step of the reverse transformation (t=16 ms), another retransformed region appears later (for X/L close to 1 and t=17.5 ms). This is also clearly visible in the temperature map of the Fig. 18(c), in which a new temperature gradient appears at point 11 for longitude x=0.

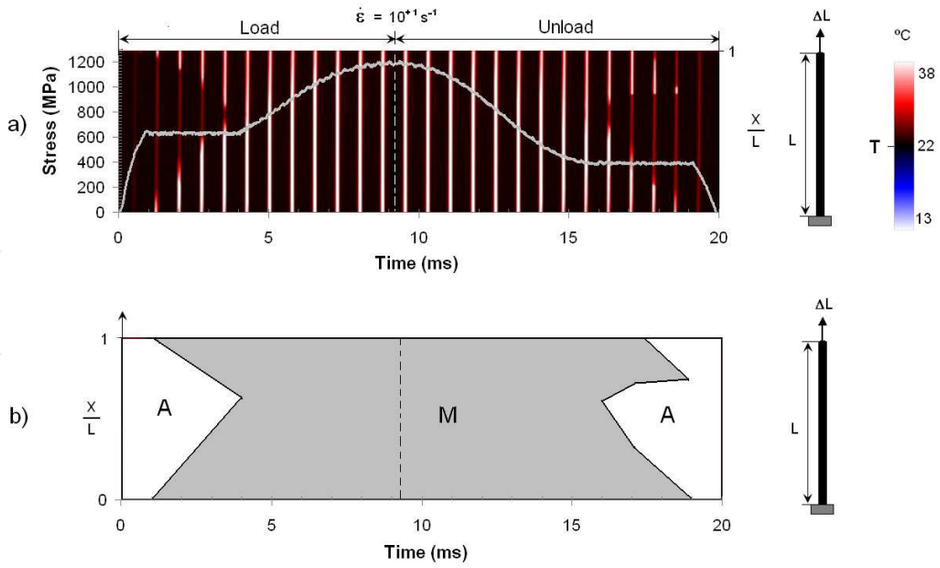

Fig. 17. a) Simultaneous evolution of the phase transformation fronts and the stress during an impact test (ε_{max}=10%), b) schematic phase diagram A(austenite)-M (martensite).

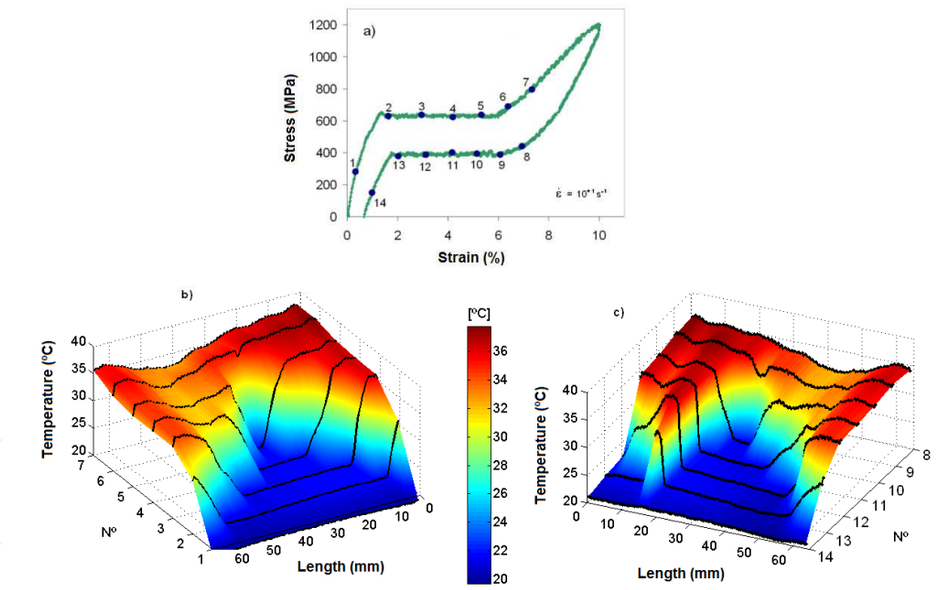

Fig. 18. Evolution of the elasto-plastic deformation of the stress induced martensitic phase at impact strain rates, a) stress-strain diagram, b) temperature evolution during the forward transformation, b) temperature evolution during the reverse transformation.

5.1 Phase transformation fronts evolution as function of the strain rate

In this section the homogeneity of the B2-B19′ martensitic transformation is discussed as function of the strain rate. This quality may be evaluated in terms of the number of the B19′ phase nucleations.

It is well known that this transformation is inhomogeneous at strain rates lower than 10^{-4} s^{-1} (Shaw & Kyriakides, 1995). The trend observed in the literature shows that the number of phase transformation fronts is multiplied as the strain rate is increase within the range from 10^{-4} s^{-1} to 10^{-2} s^{-1} (Shaw & Kyriakides, 1995; Chang et al., 2006), going against the results obtained in the previous section at impact strain rates, 10^{+1} s^{-1}, where the transformation appears to be inhomogeneous, without multiple transformation fronts. In order to study in depth this evolution, the number of nucleations was observed at intermediate strain rates.
In fact, when the strain rate is low enough, only phase transformation fronts nucleated at grips are observed, Fig. 19. Once the nucleation takes place, the stress necessary to its propagation is lower than that necessary to originate a new nucleation, so that the initial front propagates leading to an inhomogeneous transformation as is corroborated in literature (Shaw & Kyriakides, 1995).

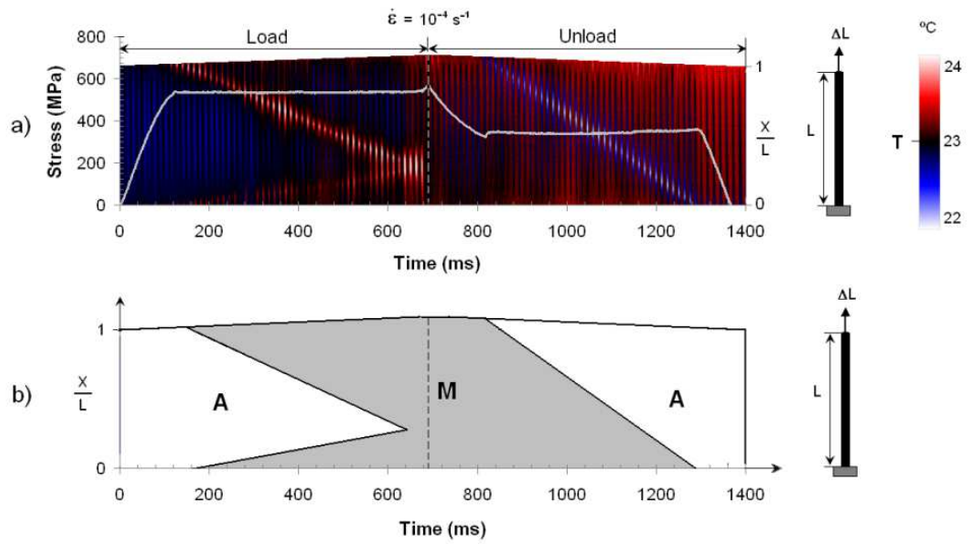

Fig. 19. a) Simultaneous evolution of the phase transformation fronts and the stress at a strain rate of 10^{-4} s^{-1}, b) schematic phase diagram A(austenite)-M (martensite).

At higher strain rates, the temperature increases in the transformed zones, since the time available to release the transformation heat to the sourrandings is reduced. This local rise of temperature increases the stress necessary for the propagation of the active front due to the inherent sensibility of this transformation with the temperature. When the strain rate is high enough, the temperature may reach such a high value that the propagation stress of the active front is higher than that necessary to allow another nucleation in a cooler region of the sample far away of the active front, so another nucleations may arise, Fig. 20.

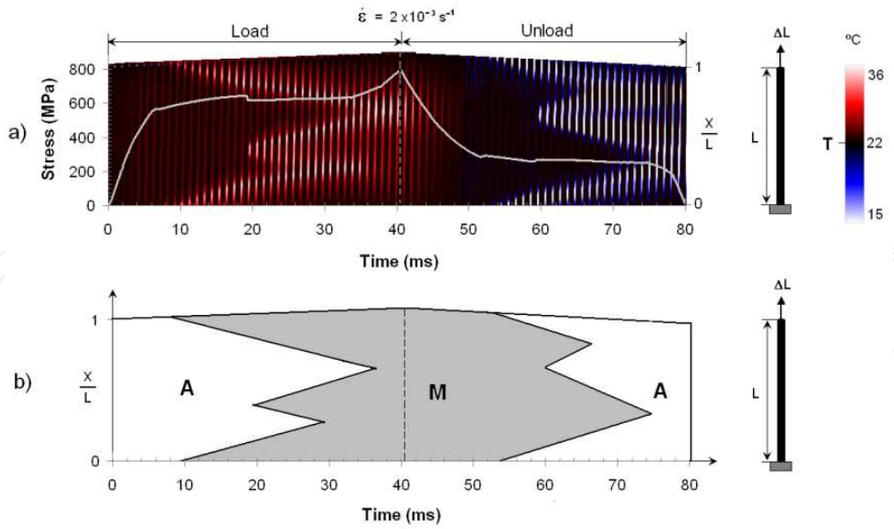

Fig. 20. a) Simultaneous evolution of the phase transformation fronts and the stress at a strain rate of $2x10^{-3}$ s^{-1}, b) schematic phase diagram A(austenite)-M (martensite).

As the strain rate increases, this effect is accentuated, and additional nucleations appear, Fig. 21. Moreover, just at the moment at which the new nucleations appear, a small drop in stress is shown, similarly to that observed in other works (Leo et al., 1993, Shaw & Kyriakides, 1997, Chang et al., 2006). This is due to the sudden and localized small increase of strain which occurs at the nucleation sites. On the other hand, the multiplication of the nucleations implies a reduction of the fronts speed in order to maintain the consistency of the global strain rate, resulting in a lower self-heating. This reduces the immediate possibility of the emergence of a new nucleation, which is postponed until the material is reheated.

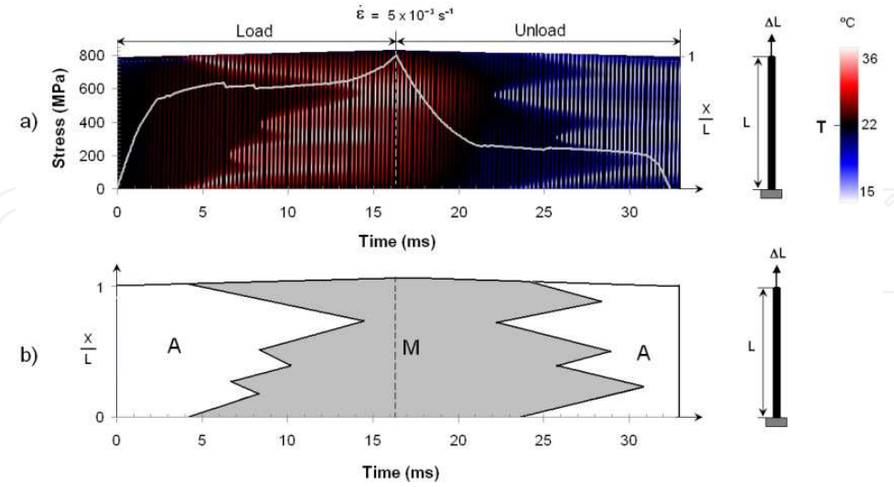

Fig. 21. a) Simultaneous evolution of the phase transformation fronts and the stress at an strain rate of $5x10^{-3}$ s^{-1}, b) schematic phase diagram A(austenite)-M (martensite).

As the strain rate increases, the time available for releasing the transformation heat to the surroundings is more and more reduced. This enhances the effect of the self-heating, and the

number of nucleations continues multiplying. In this case, the temperature at the beginning of the reverse transformation may be even greater than the initial temperature of the specimen, Fig. 22.

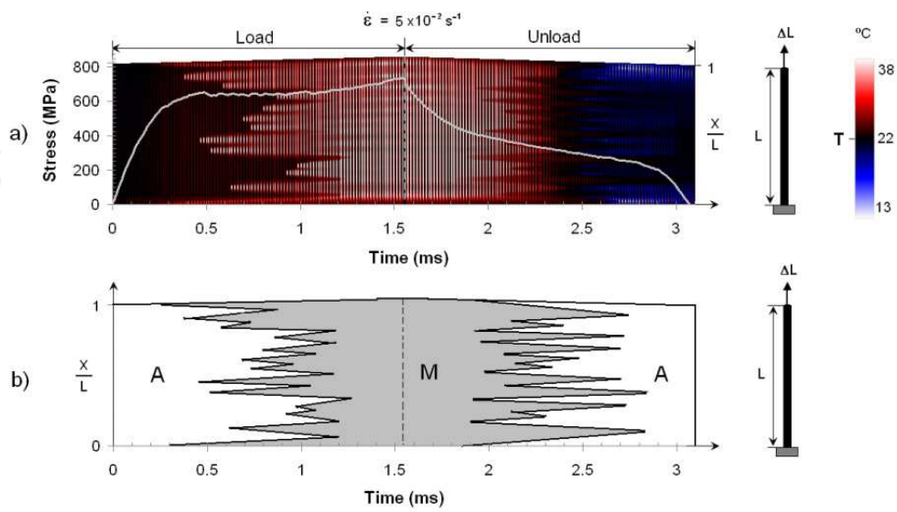

Fig. 22. a) Simultaneous evolution of the phase transformation fronts and the stress at an strain rate of $5x10^{-2}$ s^{-1}, b) schematic phase diagram A(austenite)-M (martensite).

Nevertheless, when the strain rate is high enough, 10^{-1} s^{-1}, the new nucleations appear near the active fronts, as is shown in Fig. 23. This may mean that at impact, Fig. 15 and Fig. 17, multiple transformations also occur, but so near the active fronts that they may are visible as a single one.

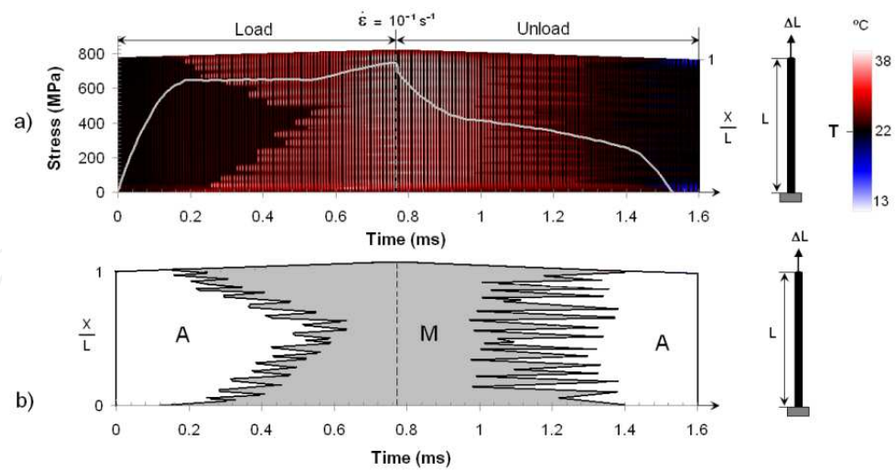

Fig. 23. a) Simultaneous evolution of the phase transformation fronts and the stress at a strain rate of 10^{-1} s^{-1}, b) schematic phase diagram A(austenite)-M (martensite).

6. References

Adharapurapu, R.R.; Jiang, F.; Vecchio, K.S. & Gray III, G.T. (2006). Response of NiTi shape memory alloy at high strain rate: A systematic investigation of temperature effects on tension-compression asymmetry. Acta Materialia, v 54, n 17, p 4609–4620.

Auricchio, F.; Faravelli, L.; Magonette, G. & Torra, V. (2001). Shape Memory Alloys. Advances in Modelling and Applications, CIMNE, Barcelona.

Boyce, B.L. & Crenshaw, T.B. (2005). Servohydraulic Methods for Mechanical Testing in the Sub-Hopkinson Rate Regime up to Strain Rates of 500 1/s. SAND2005-5678, Sandia National Laboratories.

Bragov, A.M.; Lomunov, A.K. & Sergeichev, I.V. (2006). High-speed behavior of some shape memory alloys. AIP Conference Proceedings, v 845, n 1, p 705–708.

Chang, B.C.; Shaw, J.A. & Iadicola, M.A. (2006). Thermodynamics of shape memory alloy wire: Modeling, experiments, and application. Continuum Mechanics and Thermodynamics, v 18, n 1–2, p 83–118.

Chen, W.W.; Wu, Q.; Kang, J.H. & Winfree, N.A. (2001). Compressive superelastic behavior of a NiTi shape memory alloy at strain rates of 0.001–750 s–1. International Journal of Solids and Structures, v 38, n 50–51, p 8989–8998.

Chrysochoos, A.; Lobel, M. & Maisonneuve, O. (1995). Thermo-mechanical coupling of pseudoelastic behaviour of CuZnAl and NiTi alloys. Comptes Rendus de l'Academie des Sciences, Serie II (Mecanique–Physique–Chimie–Astronomie), v 320, n 5, p 217–223.

Dolce, M. & Cardone, D. (2001). Mechanical behaviour of shape memory alloys for seismic applications 2. Austenite NiTi wires subjected to tension. International Journal of Mechanical Sciences, v 43, n 11, p 2657–2677.

Duerig, T.W.; Melton, K.N.; Stöckel, D. & Wayman, C.M. (1990). Engineering aspects of shape memory alloys, Butterworth– Heinemann, London.

Entermeyer, D.; Patoor, E.; Eberhardt, A. & Berveiller, M. (2000). Strain rate sensitivity in superelasticity. International Journal of Plasticity, v 16, n 10–11, p 1269–1288.

Funakubo, H. (1987). Application of shape memory alloys, In: Shape Memory Alloys, Funakubo, H. & Kennedy J.B. (Eds.), second ed., pp. 227–269, Gordon and Breach Science, New York.

Iadicola, M.A. & Shaw, J.A. (2007). An experimental method to measure initiation events during unstable stress–induced martensitic transformation in a shape memory alloy wire. Smart Materials and Structures, v 16, n 1, p 155–169.

Lagoudas, D.C., (2008). Shape Memory Alloys: Modeling and Engineering Applications, Spriger, University College Station TX, USA.

Leo, P.H.; Shield, T.W. & Bruno, O.P. (1993). Transient heat transfer effects on the pseudoelastic behavior of shape-memory wires. Acta Metallurgica et Materialia, v 41, n 8, p 2477-2485.

Li, H., Mao, C.; Ou, J. (2005). Strain self–sensing property and strain rate dependent constitutive model of austenitic shape memory alloy: Experiment and theory. Journal of Materials in Civil Engineering, v 17, n 6, p 676–685.

Lin, P.H.; Tobushi, H.; Tanaka, K.; Hattori, T. & Ikai, A. (1996). Influence of strain rate on deformation properties of TiNi shape memory alloy. JSME International Journal, Series A, v 39, n 1, p 117–123.

Liu, Y., Li, Y., Xie, Z. & Ramesh, K.T. (2002). Dynamic deformation of shape- memory alloys: evidence of domino detwinning? Philosophical Magazine Letters, v 82, n 9, p 511–517.

Miller, D.A.; Thissell, W.R. & Macdougall, D.A.S. (2000). Dynamic tensile plasticity and damage evolution in shape–memory Ni–Ti. Journal de Physique IV, v 10, n 9, p 341–346.

Niemczura, J. & Ravi-Chandar, K. (2006). Dynamics of propagating phase boundaries in NiTi. Journal of the Mechanics and Physics of Solids, v 54, n 10, p 2136–2161.

Otsuka, K. & Wayman, C.M. (1998). Shape Memory Materials. Cambridge Unversity Press, Cambridge.

Pieczyska, E.A.; Tobushi, H.; Gadaj, S.P. & Nowacki, W.K. (2006a). Superelastic deformation behaviors based on phase transformation bands in TiNi shape memory alloy. Materials Transactions, v 47, n 3, p 670–676.

Pieczyska, E.A.; Gadaj, V.; Nowacki, W.K. & Tobushi, H. (2006b). Phase–transformation fronts evolution for stress– and strain–controlled tension tests in TiNi shape memory alloy. Experimental Mechanics, v 46, n4, 531–542.

Pieczyska, E.; Nowacki, W.; Sakuragi, T. & Tobushi, H. (2007). Superelastic deformation properties of TiNi shape memory alloy. Key Engineering Materials, 340–341, pt.2, p 1211–1216.

Prahlad, H. & Chopra, I. (2000). Experimental characterization of Ni–Ti shape memory alloy wires under uniaxial loading conditions. Journal of Intelligent Material Systems and Structures, v 11, n 4, p 272–282.

Qiu, Z.–X.; Yao, X.T.; Yuan, J. & Soutis, C. (2006). Experimental research on strain monitoring in composite plates using embedded SMA wires. Smart Materials and Structures, v 15, n 4, p 1047–1053.

Schmidt, I. (2006). A phenomenological model for superelastic NiTi wires based on plasticity with focus on strain–rate dependency caused by temperature. Transactions of the ASME. Journal of Engineering Materials and Technology, v 128, n 3, p 279–284.

Shaw, J.A. & Kyriakides, S. (1995). Thermo-mechanical aspects of NiTi. Journal of the Mechanics and Physics of Solids, v 43, n 8, p 1243–1281.

Shaw, J.A. & Kyriakides, S. (1997). On the nucleation and propagation of phase transformation fronts in a NiTi alloy. Acta Materialia, v 45, n 2, p 683–700.

Tobushi, H.; Shimeno, Y.; Hachisuka, T. & Tanaka, K. (1998). Influence of strain rate on superelastic properties of TiNi shape memory alloy. Mechanics of Materials, v 30, n 2, p 141–150.

Tsoi, K.A., Stalmans, R., Schrooten, J., Wevers, M. & Mai, Y. (2003). Impact damage behaviour of shape memory alloy composites. Materials Science & Engineering A, v A342, n 1-2, p 207–215.

Vitiello, A.; Giorleo, G. & Morace, R.E. (2005). Analysis of thermo-mechanical behaviour of Nitinol wires with high strain rates. Smart Materials and Structures, v 14, n 1, p 215–221.

Wu, K,; Yang, F.; Pu, Z. & Shi, J. (1996). Effect of strain rate on detwinning and superelastic behavior of NiTi shape memory alloys. Journal of Intelligent Material Systems and Structures, v 7, n 2, p 138–144.

Xu, R.; Cui, L. & Zheng, Y. (2006). The dynamic impact behavior of NiTi alloy. Materials Science and Engineering A, v 438-440, n SPEC. ISS., p 571-574.

Zurbitu, J.; Castillo, G.; Urrutibeascoa, I. & Aurrekoetxea, J. (2009a). Low–energy tensile–impact behavior of superelastic NiTi shape memory alloy wires. Mechanics of Materials, v 41, n 9, p 1050–1058.

Zurbitu, J.; Castillo, G.; Aretxabaleta, L. & Aurrekoetxea, J. (2009b). Phase transformation fronts propagation during the Stress Induced Martensitic transformation in NiTi Shape Memory Alloy wires at impact strain rates. ESOMAT 2009 - The 8th European Symposium on Martensitic Transformations, [06038], edited by P. Šittner, L. Heller and V. Paidar, published by EDP Sciences.

Zurbitu, J.; Kustov, S.; Castillo, G.; Aretxabaleta, L.; Cesari, E. & Aurrekoetxea, J. (2009c). Instrumented tensile–impact test method for shape memory alloy wires. Materials Science and Engineering A, v 524, n 1–2, p 108–111.

IntechOpen

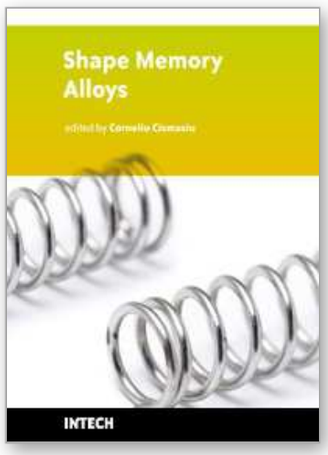

Shape Memory Alloys

Edited by Corneliu Cismasiu

ISBN 978-953-307-106-0
Hard cover, 210 pages
Publisher Sciyo
Published online 18, October, 2010
Published in print edition October, 2010

In the last decades, the Shape Memory Alloys, with their peculiar thermo-mechanical properties, high corrosion and extraordinary fatigue resistance, have become more popular in research and engineering applications. This book contains a number of relevant international contributions related to their properties, constitutive models and numerical simulation, medical and civil engineering applications, as well as aspects related to their processing.

How to reference

In order to correctly reference this scholarly work, feel free to copy and paste the following:

Javier Zurbitu, Sergey Kustov, Ane Zabaleta, Eduard Cesari and Jon Aurrekoetxea (2010). Thermo-Mechanical Behaviour of NiTi at Impact, Shape Memory Alloys, Corneliu Cismasiu (Ed.), ISBN: 978-953-307-106-0, InTech, Available from: http://www.intechopen.com/books/shape-memory-alloys/thermo-mechanical-behaviour-of-niti-at-impact

INTECH
open science | open minds

InTech Europe
University Campus STeP Ri
Slavka Krautzeka 83/A
51000 Rijeka, Croatia
Phone: +385 (51) 770 447
Fax: +385 (51) 686 166
www.intechopen.com

InTech China
Unit 405, Office Block, Hotel Equatorial Shanghai
No.65, Yan An Road (West), Shanghai, 200040, China
中国上海市延安西路65号上海国际贵都大饭店办公楼405单元
Phone: +86-21-62489820
Fax: +86-21-62489821

IntechOpen